Biophysical Journal, Volume *112*

Supplemental Information

Ephemeral Protein Binding to DNA Shapes Stable Nuclear Bodies and Chromatin Domains

Chris A. Brackley, Benno Liebchen, Davide Michieletto, Francois Mouvet, Peter R. Cook, and Davide Marenduzzo

Ephemeral protein binding to DNA shapes stable nuclear bodies and chromatin domains: Supporting Information

C. A. Brackley, B. Liebchen, D. Michieletto, F. Mouvet, P. R. Cook, and D. Marenduzzo

Here we give more details on the simulations (including parameter values), and on the continuum mean field model (derivation, linear stability analysis and amplitude equation); we also show additional results and figures which are discussed in the main text.

I. DETAILS OF BROWNIAN DYNAMICS SIMULATIONS

The chromatin fiber is modeled as a bead-spring polymer with finitely-extensible non-linear elastic springs via a Kremer-Grest model [1]. To map length scales from simulation to physical units, we can, e.g., set the diameter, σ, of each bead to ~ 30nm$\simeq 3$ kbp (assuming an underlying 30 nm fiber; of course, all our results would remain valid with a different mapping).

Letting $\boldsymbol{r}_i$ and $\boldsymbol{d_{i,j}} \equiv \boldsymbol{r}_j - \boldsymbol{r}_i$ be respectively the position of the centre of the i-th bead and the vector of length $d_{i,j}$ between beads i and j, we can express the potential modeling the connectivity of the chain as

$$U_{\mathrm{FENE}}(i,i+1) = -\frac{k}{2}R_0^2 \ln\left[1-\left(\frac{d_{i,i+1}}{R_0}\right)^2\right],$$

for $d_{i,i+1} < R_0$ and $U_{\mathrm{FENE}}(i,i+1) = \infty$, otherwise; here we chose $R_0 = 1.6\ \sigma$ and $k = 30\ k_BT/\sigma^2$.

The bending rigidity of the chain is described through a standard Kratky-Porod potential, as follows

$$U_b(i,i+1,i+2) = \frac{k_BTl_p}{\sigma}\left[1-\frac{\boldsymbol{d}_{i,i+1}\cdot\boldsymbol{d}_{i+1,i+2}}{d_{i,i+1}d_{i+1,i+2}}\right],$$

where we set the persistence length $l_p = 3\sigma \simeq 90$ nm, which is reasonable for a chromatin fiber.

The steric interaction between a chromatin bead, a, and a protein bridge, b (of sizes $\sigma_a = \sigma_b = \sigma$), is modeled through a truncated and shifted Lennard-Jones potential

$$U_{\mathrm{LJ}}(i,j) = 4\epsilon_{ab}\left[\left(\frac{\sigma}{d_{i,j}}\right)^{12} - \left(\frac{\sigma}{d_{i,j}}\right)^{6} - \left(\frac{\sigma}{r_c}\right)^{12} + \left(\frac{\sigma}{r_c}\right)^{6}\right],$$

for $d_{i,j} < r_c$ and 0 otherwise. This parameter, r_c, is the interaction cutoff; it is set to $r_c = 2^{1/6}\sigma$ for inactive proteins, in order to model purely repulsive interactions, and to $r_c = 1.8\sigma$ for an active protein, so as to include attractive interactions. In both cases, the potential is shifted to zero at the cut-off in order to have a smooth curve and avoid singularities in the forces. Purely repulsive interactions, such as those between inactive proteins and chromatin segments, are modeled by setting $\epsilon_{ab} = k_BT$, while attractive interactions are modeled using: (i) $\epsilon_{ab} = 3k_BT$ (for non-specific interactions, Fig. 1); (ii) $\epsilon_{ab} = 15k_BT$ and $\epsilon_{ab} = 4k_BT$ (for non-specific and specific interactions respectively, Fig. 3); (iii) $\epsilon = 4k_BT$ (for non-specific interactions, Fig. 4); or (iv) as specified in Supporting Figure captions in other cases.

The total potential energy experienced by bead i is given by

$$\begin{aligned} U_i \;=\; & \sum_j U_{\mathrm{FENE}}(i,j)\delta_{j,i+1} + \\ & \sum_j\sum_k U_{\mathrm{b}}(i,j,k)\delta_{j,i+1}\delta_{k,i+2} + \sum_j U_{\mathrm{LJ}}(i,j), \end{aligned} \tag{1}$$

and its dynamics can be described by the Langevin equation

$$m\ddot{\boldsymbol{r}}_i = -\xi\dot{\boldsymbol{r}}_i - \nabla U_i + \boldsymbol{\eta}_i, \tag{2}$$

where m is the bead mass, ξ is the friction coefficient, and $\boldsymbol{\eta}_i$ is a stochastic delta-correlated noise. The variance of each Cartesian component of the noise, σ_η^2, satisfies the usual fluctuation dissipation relation $\sigma_\eta^2 = 2\xi k_BT$.

As is customary [1], we set $m/\xi = \tau_{\rm LJ} = \tau_{\rm B}$, with the LJ time $\tau_{\rm LJ} = \sigma\sqrt{m/\epsilon}$ and the Brownian time $\tau_{\rm B} = \sigma/D_b$, where ϵ is the simulation energy unit, equal to k_BT, and $D_b = k_BT/\xi$ is the diffusion coefficient of a bead of size σ. From the Stokes friction coefficient for spherical beads of diameter σ we have that $\xi = 3\pi\eta_{sol}\sigma$ where η_{sol} is the solution viscosity. One can map this to physical units by setting the viscosity to that of the nucleoplasm, which ranges between $10 - 100$ cP, and by setting $T = 300$ K and $\sigma = 30$ nm, as above. From this it follows that $\tau_{\rm LJ} = \tau_{\rm B} = 3\pi\eta_{sol}\sigma^3/\epsilon \simeq 0.6 - 6$ ms; τ_B is our time simulation unit, used when measuring time in the figures in the main text and in this Supporting Information. The numerical integration of Eq. (2) is performed using a standard velocity-Verlet algorithm with time step $\Delta t = 0.01\tau_{\rm B}$ and is implemented in the LAMMPS engine. We perform simulations for up to 2×10^5 $\tau_{\rm B}$, which correspond to 2-20 minutes in real time. Protein switching is including by coupling an external code to LAMMPS; the external code changes stochastically type with rate α. This code is called every 1000 or 10000 LAMMPS Brownian dynamics steps, through the LAMMPS input file.

II. MEAN FIELD THEORY FOR SWITCHING PROTEINS

In our particle based simulations we observed the growth of clusters due to bridging interactions (see main text). When protein activation-inactivation reactions were absent, these clusters coarsened, resulting in one large macroscopic cluster in steady state. However, in the presence of these reactions, the clusters coarsened only up to a self-limiting size. To better understand this transition from macrophase separation to microphase separation, and the involved length scales, we now develop a phenomenological minimal model for the dynamics of chromatin and proteins. We describe the distribution of chromatin via the probability density field $\rho(\mathbf{x}, t)$, and the density of active, or binding, and inactive, or non-binding, proteins by $\Phi_a(\mathbf{x}, t) \equiv \Phi(\mathbf{x}, t)$ and $\Phi_i(\mathbf{x}, t)$ respectively.

The starting point for our model is the free energy $\mathcal{F} = \int f(\mathbf{x})\mathrm{d}\mathbf{x}$ where f is the free energy density:

$$f = \frac{D_1'}{2}\rho^2 + \frac{D_2'}{2}\Phi^2 - \chi'\rho\Phi + \frac{k'}{2}(\nabla\rho)^2 + \frac{g'}{4}\rho^4. \tag{3}$$

Here, the first two terms describe diffusion of chromatin and proteins respectively, the third term describes the energy gain through bridging and the last two terms, multiplied by k', g', respectively penalize sharp interfaces due to interfacial tension, and strong accumulations of chromatin due to short ranged repulsions.

Assuming diffusive dynamics here and using the fact that in the absence of protein modification, the number density of all species (ρ, Φ, Φ_i) is conserved, we can derive the equations of motions for our fields as done for model B dynamics [2]. However, in the presence of active protein modification, we need an additional reaction term, so that our equations of motion read

$$\dot\rho = M_\rho\nabla^2\frac{\delta\mathcal{F}}{\delta\rho}, \tag{4}$$

$$\dot\Phi_a = M_a\nabla^2\frac{\delta\mathcal{F}}{\delta\Phi_a} - \alpha\Phi_a + \beta\Phi_i. \tag{5}$$

Here M_ρ and M_a are dimensionless mobility coefficients of chromatin and activated proteins respectively, while α and β are the activation and inactivation rates for proteins. Since inactive proteins do not bind, we assume that they diffuse quickly, i.e. that their density field is uniform.

Now integrating Eq. (5) over the whole system and denoting the total number of active and inactive proteins with $N_a(t)$ and $N_i(t)$ respectively, we obtain $\dot N_a = -\alpha N_a + \beta N_i$. Conservation of the total protein number $N = N_a + N_b$ now yields $\dot N_i = (1 + \beta/\alpha)N_i$ which approaches the steady state $N_i = \alpha N/(\alpha + \beta)$, i.e. $\Phi_i = \alpha/(\alpha + \beta)$, exponentially fast. Now defining $\Phi_0 := (\beta/\alpha)\Phi_i = \beta/(\alpha + \beta)$ (and ignoring short-time effects due to possible 'imbalances' between active and inactive proteins in the initial state), Eqs. (4,5) reduce to:

$$\dot\rho = M_\rho\nabla^2[a_1\rho - k\nabla^2\rho - \chi\Phi + g\rho^3], \tag{6}$$

$$\dot\Phi = M_\Phi\nabla^2[a_2\Phi - \chi\rho] - \alpha(\Phi - \Phi_0), \tag{7}$$

where for simplicity hereon we drop the subscript a on Φ_a for active proteins. We also introduced $D_1 = M_\rho a_1$ and $D_2 = M_\Phi a_2$.

To further reduce these equations and to identify a minimal set of dimensionless control parameters, we now choose time and space units $t_u = 1/\alpha$ and $x_u = \sqrt{D_2/\alpha}$ and redefine $\Phi = \Phi\chi M_\rho/D_2$. This leads to

$$\dot\rho = \mathcal{D}_0\nabla^2\rho - A\nabla^4\rho - \nabla^2\phi + G\nabla^2\rho^3, \tag{8}$$

$$\dot\Phi = \nabla^2\Phi - X\nabla^2\rho - (\Phi - \Phi_0). \tag{9}$$

That is, our parameter space is spanned by the four dimensionless numbers $X = (\chi^2 M_\rho M_\Phi / D_2^2)$; $\mathcal{D}_0 = (D_1/D_2)$; $A = \alpha k M_\rho/(D_2^2)$ and $G = g M_\rho / D_2$.

A. Linear stability analysis

To better understand in which parameter regimes we should expect (i) a uniform distribution of chromatin and proteins, (ii) cluster growth proceeding to macroscopic phase separation and (iii) microphase separation, we now perform a linear stability analysis. This analysis will equip us with a prediction for the self-limiting cluster size in regime (iii), matching the results of our particle based simulations. We therefore study the response of the uniform phase to small perturbations in the density fields (ρ, Φ). Linearising Eqs. (8,9) around the uniform solution $(\rho, \Phi) = (\rho_0, \Phi_0)$, where ρ_0 is the DNA density as fixed by the initial state, leads to the following equations of motion for the fluctuations $\rho' = \rho - \rho_0, \Phi' = \Phi - \Phi_0$:

$$\dot{\rho}' = \mathcal{D}\nabla^2\rho' - A\nabla^4\rho - \nabla^2\Phi', \tag{10}$$

$$\dot{\Phi}' = \nabla^2\Phi' - X\nabla^2\rho' - \Phi'. \tag{11}$$

Here, we defined $\mathcal{D} := \mathcal{D}_0 + 3G\rho_0^2$. Fourier transforming Eqs. (10,11) and using $Q := \mathbf{q}^2$ leads to the following dispersion relation (or characteristic polynomial),

$$\lambda(Q) = \frac{1}{2}\Big[-1 - Q\,(1 + \mathcal{D} + AQ) \pm\sqrt{[-1 + Q(\mathcal{D} - 1 + AQ)]^2 + 4Q^2X}\Big], \tag{12}$$

which links the growth rate λ of the fluctuation with its wavevector Q. An analysis of this relation leads us to the instability criterion

$$\sqrt{X} > \sqrt{X_C} := \sqrt{A} + \sqrt{\mathcal{D}}, \tag{13}$$

which translates, in physical units, to

$$\chi > \sqrt{\frac{k\alpha}{M_\Phi}} + \sqrt{\frac{D_2}{M_\Phi}\left[\frac{D_1}{M_\rho} + 3g\rho_0^2\right]}. \tag{14}$$

This criterion determines the transition line (hypersurface) between regions (i) and (ii/iii) in the parameter space. Hence, if the bridging interactions are sufficiently large, small fluctuations around the uniform state will grow to form clusters. Remarkably, this instability and the corresponding emergence of order (clustered phase) is not contingent on the presence of a certain minimal protein (or DNA) density, suggesting that even a very low protein concentration is sufficient to trigger clustering.

To map out the transition line from macrophase separation to microseparation (at the onset of instability), it is useful to consider the wavelength at which instability first occurs. From Eq. (12) and $q_c = \partial_q \lambda(q) = 0|_{X=(\sqrt{A}+\sqrt{D})^2}$, we find $q_c = (D/A)^{1/4}$, corresponding, in physical units, to the length scale

$$L_c = \frac{2\pi}{q_c} = 2\pi\left(\frac{D_1 D_2 + 3M_\rho g\rho_0^2 D_2}{\alpha k M_\rho}\right)^{1/4}. \tag{15}$$

Thus, in an infinite system, coarsening only occurs for $\alpha = 0$. [In finite systems macrophase separation is observed if α is small enough that L_c exceeds the system size.] From this analysis we expect the average particle number per cluster to scale as $N \propto L_c^3 \propto \alpha^{-3/4}$ (at least close to the onset of instability). This value agrees well with the numerically observed scaling of $N \propto \alpha^{-0.76}$ (Fig. 2B), supporting the view that the essential physics of chromatin clustering can be described and understood within our simplified mean field theory.

For completeness, we also calculate the boundaries of the instability band from Eq. (12), which, after translating back into physical units (for $M_1 = M_2 = 1$), read as follows:

$$q_\pm = \frac{1}{\sqrt{2D_2K}}\sqrt{\nu \pm \sqrt{\nu^2 - 4D_2K\alpha(D_1 + 3g\rho_0^2)}}, \tag{16}$$

$$\nu = \left[\chi^2 - D_1D_2 - 3D_2g\rho_0^2 - K\alpha\right]. \tag{17}$$

At the onset of instability, we find $\nu \to 4D_2K\alpha(D_1 + 3g\rho_0)$ and hence we recover the $\alpha^{1/4}$-scaling of the onset mode. In contrast, the boundaries of the instability band scale in a more complicated way which is nonuniversal in α.

B. Amplitude equations

We now perform a perturbative analysis of the linearly unstable modes (fluctuations) close to onset of instability. This analysis will lead us to a further reduced effective model, describing the linear growth and nonlinear saturation of chromatin clusters on large scales and at long timescales.

We begin by rewriting Eqs. (4,5) as

$$\mathcal{L}\begin{pmatrix}\rho'\\ \Phi'\end{pmatrix}+\mathcal{N}-\begin{pmatrix}\dot\rho'\\ \dot\Phi'\end{pmatrix}=\begin{pmatrix}0\\0\end{pmatrix}, \tag{18}$$

where the linear operator $\mathcal{L}$ and the nonlinear term $\mathcal{N}$ represent

$$\mathcal{L}=\begin{pmatrix}\mathcal{D}\partial_x^2-A\partial_x^4 & -\partial_x^2\\ -X\partial_x^2 & \partial_x^2-1\end{pmatrix};\quad \mathcal{N}=G\begin{pmatrix}\partial_x^2\rho'^3+3\rho_0\partial_x^2\rho'^2\\ 0\end{pmatrix}. \tag{19}$$

Now, we replace (as usual, see [3])

$$X\to(1+\epsilon)X_C;\quad \partial_x\to\partial_x+\sqrt{\epsilon}\partial_X;\quad \partial_t\to\epsilon\partial_T \tag{20}$$

where $\epsilon=(X-X_C)/X_C$ and expand the fields as

$$\rho'=\sum_{n=1}^{\infty}\epsilon^{n/2}\rho_{n-1};\quad \Phi'=\sum_{n=1}^{\infty}\epsilon^{n/2}\Phi_{n-1}. \tag{21}$$

Next, we plug these expansions into Eqs. (19) and solve the resulting equations to lowest order ($\epsilon^{1/2}$). Using the Ansatz $\rho_0=\mathcal{A}\exp(\mathrm{i}q_cx)+c.c.$ and $\Phi_0=\mathcal{A}_\phi\exp(\mathrm{i}q_cx)+c.c.$ with amplitudes $\mathcal{A},\mathcal{A}_\phi$, we find $q_c=(\mathcal{D}/A)^{1/4}$ reproducing the corresponding result from our linear stability analysis (see above), as well as $\mathcal{A}_\phi=\mathcal{A}(\mathcal{D}+Aq_c^2)=\mathcal{A}\sqrt{\mathcal{D}X_C}$ which fixes the relation between the amplitudes of both density fields. The solution of our perturbative equations to order $\epsilon^{1/2}$ then reads $\rho'=2\mathcal{A}\cos q_cx$ with the so-far unknown amplitude $\mathcal{A}$.

The result to order ϵ turns out not to be particular useful for our purpose, as solving it would provide us with a similar result as to order $\epsilon^{1/2}$), but with another unknown amplitude $\mathcal{A}'$ yielding a higher order correction to the solution $\rho'=2\mathcal{A}\cos q_cx$. Since we are looking only for the lowest order result in ϵ we directly consider the perturbative equations of motion to order $\epsilon^{3/2}$. As usual [3], we do not attempt to solve the corresponding equations explicitly, but apply Fredholm's theorem providing solvability conditions, which determine an equation of motion for $\mathcal{A}$. After a long but straightforward calculation and transforming back to coordinates t,x we find:

$$c_t\dot{\mathcal{A}}=\epsilon\mathcal{A}+c_x\partial_x^2\mathcal{A}+c_3\mathcal{A}^3, \tag{22}$$

where

$$c_t = \sqrt{\frac{A}{X_C}}\left(1+\frac{1}{\mathcal{D}}\right), \tag{23}$$

$$c_x = \frac{4A}{\sqrt{\mathcal{D}X_C}}, \tag{24}$$

$$c_3 = \frac{3G}{\sqrt{\mathcal{D}X_C}}. \tag{25}$$

Eq. (22) is a variant of the real Ginzburg-Landau equation, here describing, together with the coefficients Eqs. (23–25), the dynamics of chromatin and proteins close to the onset of instability. In this equation $\epsilon/(c_tt_u)$ is the initial growth rate of protein clusters; $x_u\sqrt{\epsilon/c_3}$ describes the amplitude of their saturation (related to their density) for a given $X>\left[\sqrt{A}+\sqrt{\mathcal{D}}\right]^2$ and $x_u\sqrt{c_x}$ is a correlation length, describing a scale of spatial modulations of the saturation amplitude of DNA clusters.

Although we equipped our original equilibrium model with reaction terms which drive it out of equilibrium, its large scale and long time dynamics (i.e., Eq. (22)) can be effectively mapped (at least close to onset of instability) onto a potential system with the following Lyapunov functional:

$$\mathcal{V}[\mathcal{A}]=\int\mathrm{d}x\left[-\epsilon|\mathcal{A}|^2+\frac{c_3}{2}|\mathcal{A}|^4+c_x^2|\partial_X\mathcal{A}|^2\right], \tag{26}$$

$$\dot{\mathcal{A}} = -\frac{1}{c_T}\frac{\delta V}{\delta \mathcal{A}}. \tag{27}$$

Hence, quite remarkably, the dynamics of the present reaction-diffusion system can be mapped, within this approximation, onto a system which is purely relaxational.

III. ADDITIONAL SIMULATION RESULTS

In this section we present additional simulation results, which complement those discussed in the main text.

Figure S1 shows that the FRAP signal (following simulated photobleaching of a spherical spot of size 50 σ) shows recovery also for equilibrium bridges, if the specific and non-specific interactions are carefully tuned. However, protein modification provides a more robust way to achieve this, which simultaneously allows stable binding (when the protein is in the active state), and fast turnover (due to the unbinding and diffusion of inactive proteins).

Figure S2 shows the cluster size for different parameter values for the case of non-specific protein-chromatin interactions. This demonstrates that it can be varied significantly (by about an order of magnitude), and is particularly sensitive to the protein concentration.

Figures S3 and S4 highlight some further properties of the recycling clusters. In particular, Figure S3 shows that these clusters retain memory of their shape even as the proteins which constitute them change. Figure S4 shows the dynamics of some protein and chromatin beads with and without modification. Without modification, once proteins bind to a cluster they diffuse little for the rest of the simulation, whereas with modification they sample the whole simulation domain. Contrary to this, the dynamics of the chromatin beads within a cluster is similar with and without modification: they diffuse very little. This explains why clusters keep their shape: while proteins bind and unbind, the underlying chromatin backbone is largely unchanged.

Finally, Figure S5 shows how the effect of protein switching on the ratio between non-local and local contacts, shown in Figure 4 in the main text, is affected by the values of non-specific and specific interactions.

IV. ESTIMATES OF RELEVANT TIMESCALES

Here we provide a series of simple estimates for the value of the relevant timescales in our problems. Consider first a fluorescence-recovery-after-photobleaching, or FRAP, experiment, where a cluster of size $\sigma_{\rm cl} \sim 0.1 - 1$ μm is inside the bleached spot, which we imagine has a diameter of $\sigma_{\rm FRAP} \sim 1$ μm. In this Section, as previously, σ will instead denote the size of a typical chromatin-binding complex, or chromatin bead (as previously, we imagine this is ~ 30 nm).

What is the timescale for the recovery of the FRAP signal? Clearly, this depends on the underlying dynamics of the bleached/unbleached proteins. If proteins diffuse freely, then unbleached proteins can enter the bleach spot to give recovery within a time, $\tau_{\rm diff}$, proportional to

$$\tau_{\rm diff} \sim \frac{\sigma^2_{\rm FRAP}}{D}. \tag{28}$$

For a protein size $\sigma \sim 30$ nm, and if the nucleoplasm viscosity is 10 cP (ten times that of water), the diffusion coefficient is $\sim 1.4\mu{\rm m}^2$ s-1, so that $\tau_{\rm diff} \sim 1$s, which is too fast to account for FRAP response of nuclear bodies (furthermore, of course, freely diffusing proteins could not self-organise into clusters).

If, instead, non-switching binding proteins create a cluster, then the FRAP signal recovers when some proteins unbind, and others replace these from the soluble (unbleached) pool. As the former process is slower than the latter (which relies again on diffusion), we can equate the FRAP recovery timescale to the time needed for an equilibrium protein to unbind from the cluster, which can be estimated as,

$$\tau_{\rm non-switch} \sim \frac{\sigma^2_{\rm cl}}{D}\exp\left(\frac{\Delta U}{k_B T}\right) \tag{29}$$

where ΔU indicates the strength of chromatin-protein interaction. If we assume an interaction of 10 kcal/mol, consistent with either multiple non-specific or a single specific DNA-protein interactions, then $\tau_{\rm non-switch} > 10^5$ s, which is too slow to account for the FRAP recovery observed in nuclear bodies. Clearly, changing ΔU will change $\tau_{\rm non-switch}$, but in order for the estimate to be in the observed range, the interaction energy would have to be finely tuned, and would be significantly lower than that seen in typical DNA-protein interactions.

If, finally, switching proteins are in the cluster, then the unbinding time, which again can be equated to the FRAP recovery time, is simply

$$\tau_{\rm switch} \sim \alpha^{-1}. \tag{30}$$

For typical post-translational modification, or transcription termination, this is in the several seconds to minutes timescale, which is compatible with experimental results.

Aside from FRAP, another important timescale is that over which local TADs form (e.g., in Fig. 4), $\tau_{\rm TAD}$. In analogy with polymer collapse and heteropolymer folding (see, e.g., Ref. [4]), we expect $\tau_{\rm TAD}$, to be a power law in the number of monomers in the TAD, say M, where the prefactor should describe microscopic (diffusion) dynamics of a monomer. Dimensional analysis then suggests

$$\tau_{\rm TAD} \sim \frac{\sigma^2}{D} M^z \sim \tau_{\rm B} M^z \tag{31}$$

where z is a scaling exponent. The Brownian time $\tau_{\rm B}$ is of the order of 10^{-3} s with previous assumptions for viscosity and monomer size, while in our simulations $z \simeq 1$ at least up to $M \sim 100$ (corresponding to 300 kbp). Also for eukaryotic chromosomes, TAD size is between 100 kbp and 1 Mbp, so M is at most a few hundred. Therefore, if $z = 1$, we estimate $\tau_{\rm TAD}$ to be of the order of 1 s, smaller than typical modification times – even assuming a larger effective value of z (e.g., $z = 2$ gives at most $\tau_{\rm TAD}$ of order of 1 min). Previous large-scale simulations also confirm that eukaryotic TADs form in minutes [5, 6]. These estimates explain why switching proteins in our simulations can still form TADs in pretty much the same way as non-switching proteins, and suggest that the same should also hold for real chromosomes.

V. CAPTIONS OF SUPPLEMENTARY MOVIES

Supplementary Movie 1: A movie of the simulation shown in Figure 1C of the main text. Proteins do not switch ($\alpha = 0$). First a snapshot 10^4 simulation units after equilibration is shown: a number of small clusters have formed. Then the subsequent dynamics are shown: clusters grow and merge, and coarsening proceeds indefinitely.

Supplementary Movie 2: A movie of the simulution shown in Figure 1D of the main text. Proteins switch at a rate $\alpha = 0.0001$ inverse Brownian times. Switching arrests coarsening, and leads to clusters of self-limiting size in steady state.

Supplementary Movie 3: Parameters for this Movie are as in Figure 3 of the main text for the $\alpha = 0$ case. Chromatin beads are not shown for simplicity. The movie starts with clusters which have formed during 10^4 simulation units following equilibration. The proteins are colored according to the cluster they belong to when the movie starts; proteins not in any clusters at that time are gray. The movie then follows the dynamics with non-switching proteins, for another 10^4 simulation units: it can be seen that colored clusters persist, therefore photobleaching such a cluster would lead to little or no recovery of signal in the cluster.

Supplementary Movie 4: As Supplementary Movie 3, but now with switching proteins ($\alpha = 0.0001$ inverse Brownian times). Proteins are colored according to the initial clusters; by the end of the simulations all clusters have mixed colors. While proteins in clusters recycle, the cluster retains the same overall shape.

Supplementary Movie 5: As in Supplementary Movie 4, but a zoom on two clusters to show more clearly clusters retain a "memory" of their shape.

Supplementary Movie 6: A movie of the simulation shown in Figure 4 in the main text. The first half of the simulation involves non-switching proteins and lasts 10^5 simulation units: two clusters form. Proteins are black; yellow chromatin beads are binding, while blue ones are non-binding. During the second half, proteins are able to switch ($\alpha = 0.0001$ inverse Brownian times); clusters split and interdomain interactions are suppressed.

[1] Kremer K., Grest G. S. (1990) Dynamics of entangled linear polymer melts: A molecular-dynamics simulation. *J. Chem. Phys.* 92(8):5057.

[2] P.M. Chaikin, P. M., Lubensky, T. C. (2000). *Principles of condensed matter physics*, Cambrdige University Press, Cambridge.
[3] Cross, M. C., Hohenberg, P. C. Pattern formation outside of equilibrium. *Rev. Mod. Phys* **65**, 851-1112 (1993).
[4] Byrne, A., Kiernan, P., Green, D., Dawson, K. A. (1995). Kinetics of homopolymer collapse. *J. Chem. Phys.* **1012**, 573-577 (1995).
[5] Michieletto, D., Marenduzzo, D., Wani, A. H. (2016) Chromosome-wide simulations uncover folding pathway and 3D organization of interphase chromosomes. arXiv:1604.03041.
[6] Brackley, C. A., Johnson, J., Kelly, S., Cook, P. R., Marenduzzo, D. (2016). Simulated binding of transcription factors to active and inactive regions folds human chromosomes into loops, rosettes and topological domains. *Nucl. Acids Res.* **44**, 3503-3512.

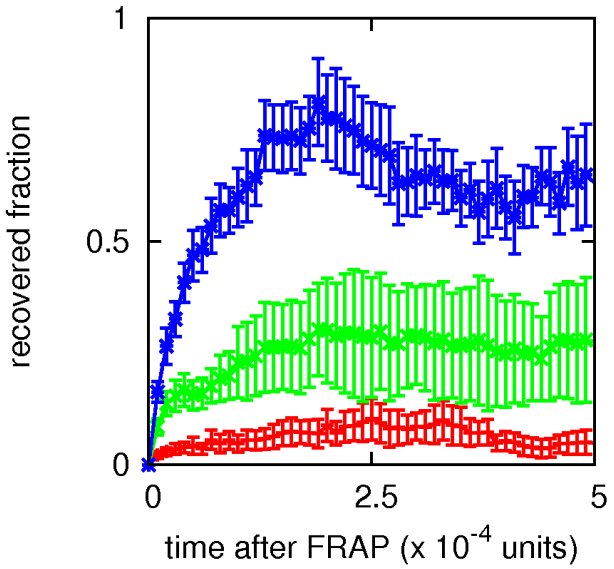

FIG. S1: **Comparison of FRAP recovery for non-switching and switching proteins**. FRAP recovery, measured as the number of unbleached proteins which are in the bleached volume after bleaching. The signals are normalized with the number of proteins in the bleached volume at the time of bleaching. As in Fig. 3Bi, the bleached volume is a sphere of size 50σ. Error bars give SD of mean, and time is given in multiples of 10^4 simulation units. Values of the specific and non-specific interactions, and of α, were respectively: $15k_BT$, $4k_BT$, 0 (red curve), $8k_BT$, $3k_BT$, 0 (green curve), and $15k_BT$, $4k_BT$, 0.0001 inverse Brownian times (blue curve). It can be seen that varying the values of non-specific and specific interactions can lead to FRAP recovery also for $\alpha = 0$ (green curve), although, in the absence of fine tuning, this is to a smaller extent with respect to $\alpha \neq 0$ (blue curve).

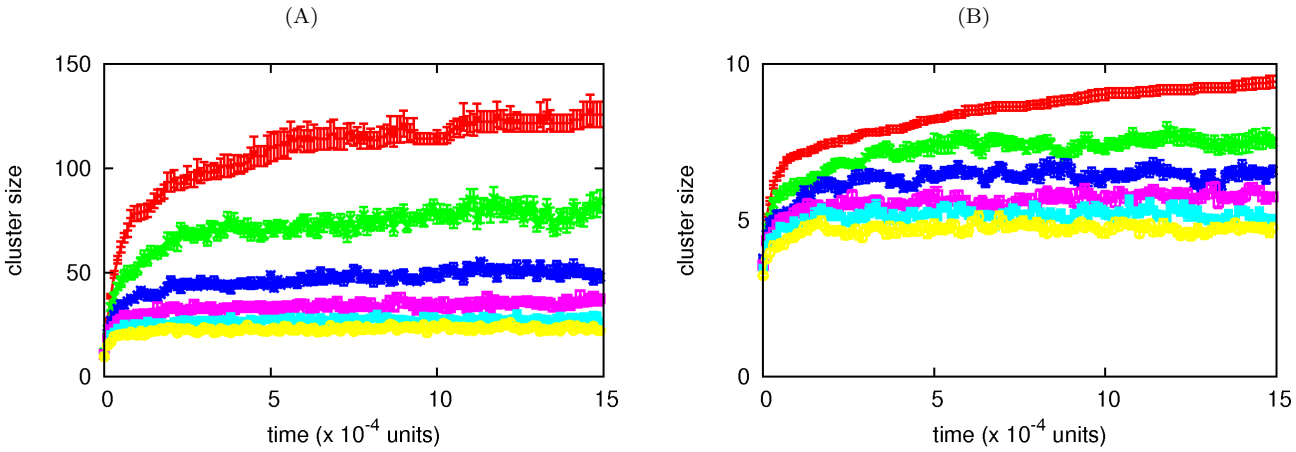

FIG. S2: **Cluster size with specific binding.** (A) Plot of the average number of proteins in a cluster versus time (± SD), for $N = 2000$ switching proteins binding to the chromatin fiber, both specifically (interaction strength 15 k_BT, cut-off 1.8σ), to every 20-th bead in the polymer, and non-specifically (interaction strength 4 k_BT, cut-off 1.8σ) to any other bead. From top to bottom, curves correspond to $\alpha = 0$ (in which case half of the proteins are non-binding, and half binding), 0.0001, 0.0002, 0.0003, 0.0004, 0.0005 respectively. (B) Same as (A), but now for $N = 500$ switching proteins, with specific interaction strength of $8k_BT$ and non-specific interaction of $3k_BT$; the interaction cut-off is 1.8σ.

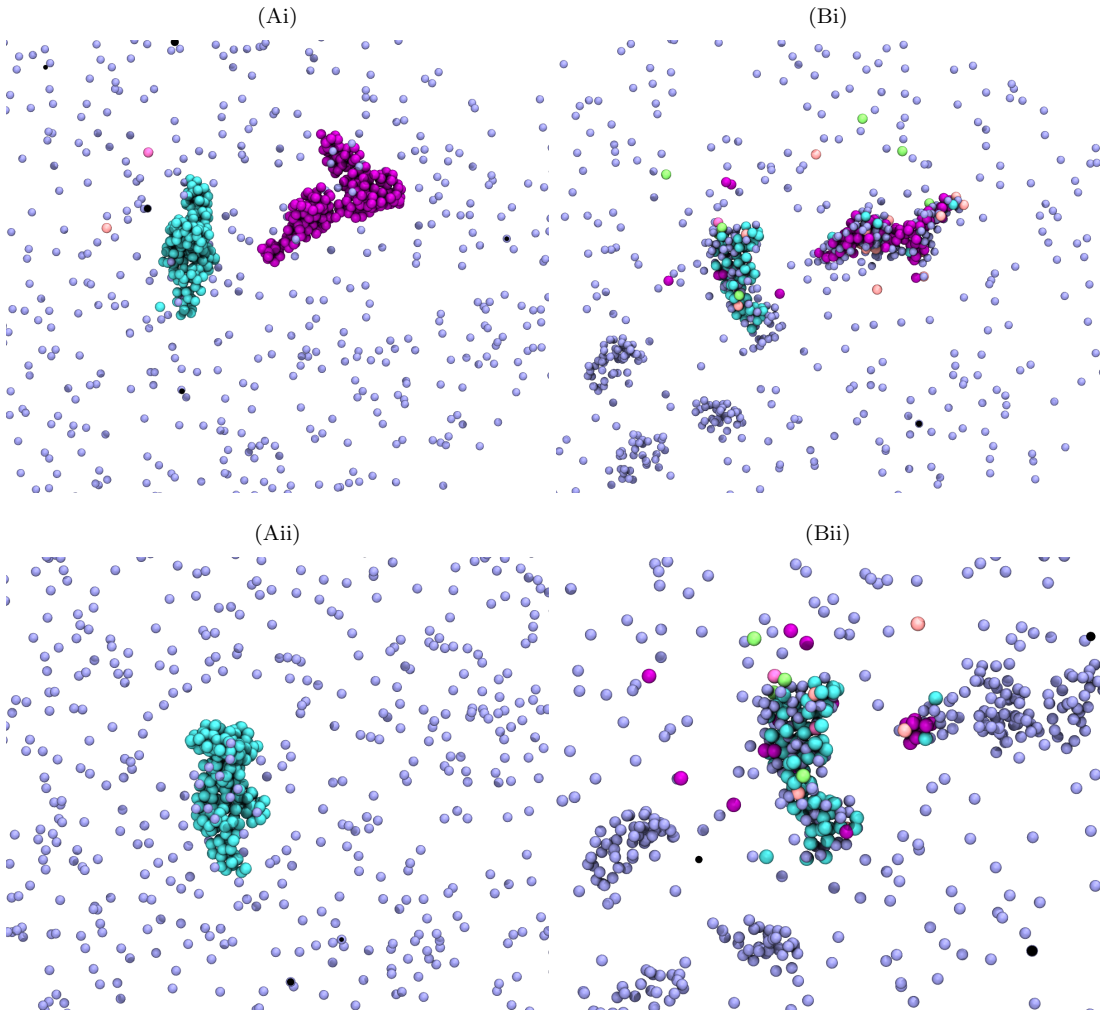

FIG. S3: **Switching proteins form clusters which retain memory of their shape.** This figure follows the evolution of clusters in a simulation analogous to that of Fig. 3A in the main text; the same parameters apply. Only proteins – and not chromatin beads – are shown for clarity. (A) Snapshots taken 10^4 time units after equilibration, for non-switching proteins, showing two clusters (beads are colored according to the cluster they belong to); (ii) shows another cluster. (B) Snapshots of the same regions shown in (A) after another 10^5 simulation units, and after allowing the proteins to now switch ($\alpha = 0.0001\tau_{\mathrm{B}}^{-1}$). Clusters recycle their constituent proteins whilst retaining a very similar shape.

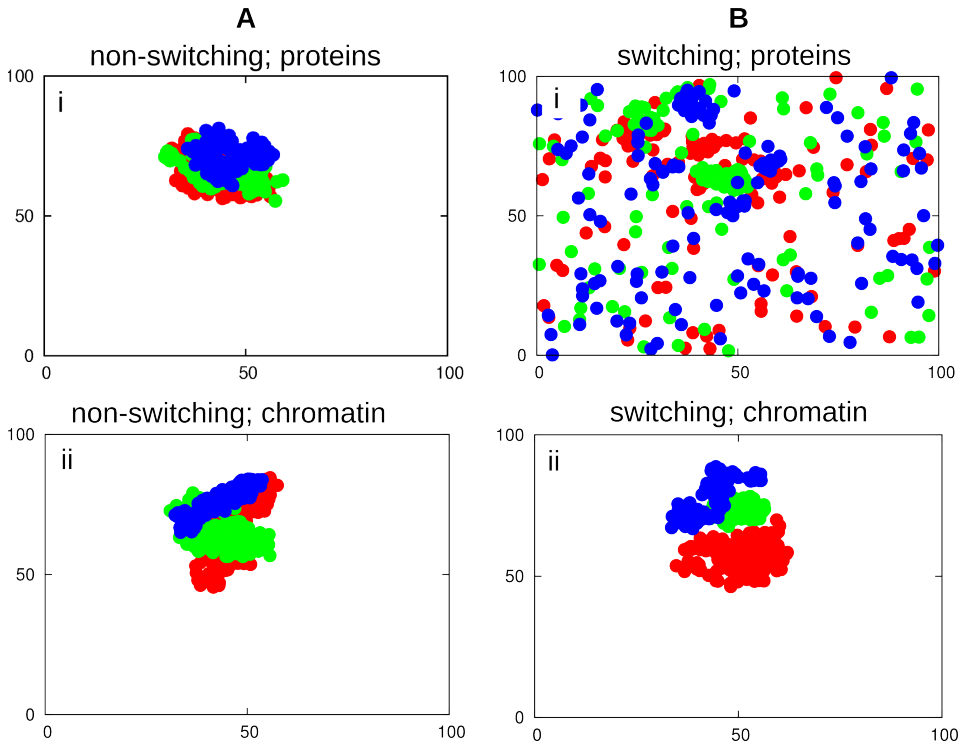

FIG. S4: **Trajectories of proteins and high-affinity chromatin beads.** Simulations are as in Fig. 3 of the main text; the same parameters apply. Positions of proteins and chromatin beads are shown in a 2D projection of the simulation domain, positions on the axes are measured in units of σ. (A) Non-switching proteins. (i) Red, green and blue circles denote positions of three non-switching proteins, recorded every 100 τ_B in a simulation (total length 1.5×10^5 simulation units. In this case, all three proteins remain bound to one cluster throughout the time series. (ii) Red, green and blue circles denote positions of three high affinity chromatin beads, again recorded every 100 τ_B in the same simulation. All three chromatin beads remain in the same cluster. (B) Same as (A), but for switching proteins ($\alpha = 0.0001$ inverse Brownian times). Now the three switching proteins diffuse through the whole space, while the three chromatin beads are still confined; this shows that the underlying scaffold of the cluster persists as the proteins are recycled.

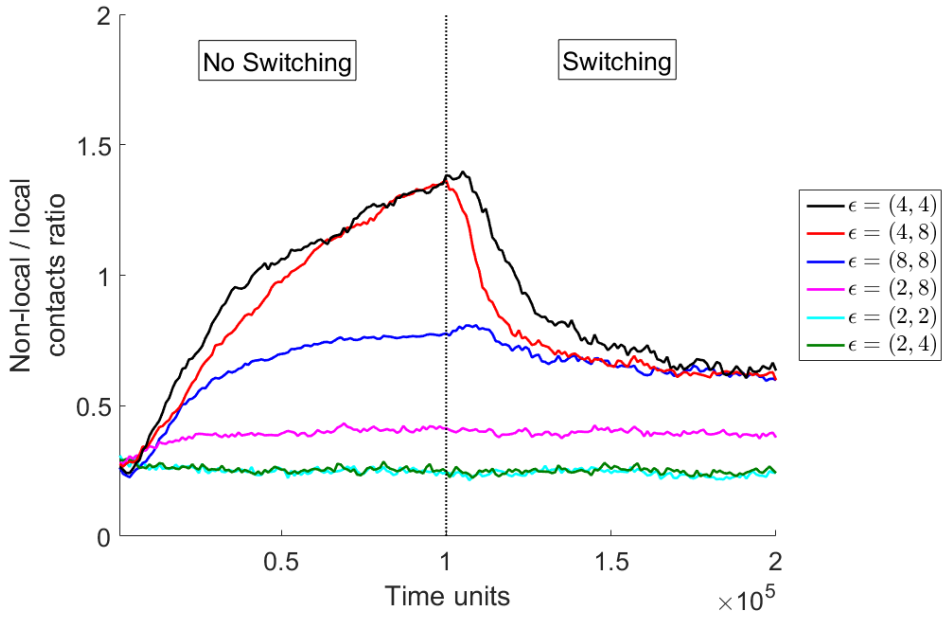

FIG. S5: **Protein switching favours local over non-local chromatin contacts.** The plot shows the fraction of non-local versus local contacts for a chromatin fiber; fiber patterning and all parameters are as in Fig. 4 of the main text. Simulations initially involved non-switching proteins; half-way through the simulation, proteins began to switch ($\alpha = 0.0001$ inverse Brownian times). Contacts are classified as local (non-local) if they involve beads separated less than (more than) 400 beads along the chain (or 1.2 Mbp. Non-specific (ϵ_1) and specific (ϵ_2) interaction energies are indicated on the right of the plot, in the format (ϵ_1, ϵ_2).